



OPEN ACCESS

EDITED BY
Wensheng Li,
Sun Yat-sen University, China

REVIEWED BY
William Ka Fai Tse,
Kyushu University, Japan
Qinghui Ai,
Ocean University of China, China

*CORRESPONDENCE
Qiyong Lou
✉ Louqiyong@ihb.ac.cn

SPECIALTY SECTION
This article was submitted to
Experimental Endocrinology,
a section of the journal
Frontiers in Endocrinology

RECEIVED 27 September 2022
ACCEPTED 30 January 2023
PUBLISHED 13 February 2023

CITATION
Liu R, Lu Y, Peng X, Jia J, Ruan Y, Shi S,
Shu T, Li T, Jin X, Zhai G, He J, Lou Q and
Yin Z (2023) Enhanced insulin activity
achieved in VDRa/b ablation zebrafish.
Front. Endocrinol. 14:1054665.
doi: 10.3389/fendo.2023.1054665

COPYRIGHT
© 2023 Liu, Lu, Peng, Jia, Ruan, Shi, Shu, Li,
Jin, Zhai, He, Lou and Yin. This is an open-
access article distributed under the terms of
the [Creative Commons Attribution License
\(CC BY\)](https://creativecommons.org/licenses/by/4.0/). The use, distribution or
reproduction in other forums is permitted,
provided the original author(s) and the
copyright owner(s) are credited and that
the original publication in this journal is
cited, in accordance with accepted
academic practice. No use, distribution or
reproduction is permitted which does not
comply with these terms.

Enhanced insulin activity achieved in VDRa/b ablation zebrafish

Ruolan Liu^{1,2}, Yao Lu¹, Xuyan Peng³, Jingyi Jia^{1,2},
Yonglin Ruan^{1,2}, Shengchi Shi^{1,2}, Tingting Shu¹, Tianhui Li¹,
Xia Jin¹, Gang Zhai¹, Jiangyan He¹, Qiyong Lou^{1*}
and Zhan Yin^{1,2,4}

¹State Key Laboratory of Freshwater Ecology and Biotechnology, Institute of Hydrobiology, Chinese Academy of Sciences, Wuhan, China, ²College of Advanced Agricultural Sciences, University of Chinese Academy of Sciences, Beijing, China, ³The Laboratory of Ophthalmology and Vision Science, Department of Ophthalmology, The First Affiliated Hospital of Zhengzhou University, Zheng Zhou, China, ⁴The Innovative Academy of Seed Design, Chinese Academy of Sciences, Beijing, China

Introduction: $1\alpha,25$ -dihydroxyvitamin D₃ ($1\alpha,25[\text{OH}]_2\text{VD}_3$) is a hormone known for its key roles in calcium absorption and nutrient metabolism. In teleost fishes, $1\alpha,25(\text{OH})_2\text{VD}_3$ insufficiency causes impaired glucose metabolism and lipid oxidation. However, the cascade and mechanisms of $1\alpha,25(\text{OH})_2\text{VD}_3$ and the vitamin d receptor (VDR) signaling are unclear.

Results: In this study, two genes (*vdra* and *vdrb*) encoding paralogs of VDRs were genetically knocked out in zebrafish. Growth retardation and accumulated visceral adipose tissue have been observed in *vdra*^{-/-};*vdrb*^{-/-} deficient line. In the liver elevated accumulation of triglycerides and suppressed lipid oxidation were detected. Moreover significantly elevated $1\alpha,25(\text{OH})_2\text{VD}_3$ levels were detected in *vdra*^{-/-};*vdrb*^{-/-} zebrafish due to *cyp24a1* transcription repression. Furthermore VDRs ablation Enhanced insulin signaling including elevated *insulin/insra* transcriptional levels, glycolysis, lipogenesis and promoted AKT/mTOR activity.

Discussion: In conclusion, our present studies provides a zebrafish model with an elevated $1\alpha,25(\text{OH})_2\text{VD}_3$ levels *in vivo*. The $1\alpha,25(\text{OH})_2\text{VD}_3$ /VDRs signaling promote lipid oxidation activity. However $1\alpha,25(\text{OH})_2\text{VD}_3$ activity of regulation of glucose homeostasis through Insulin/Insra was independent of nuclear VDRs in teleosts.

KEYWORDS

$1\alpha,25(\text{OH})_2\text{VD}_3$, VDRs, insulin, lipolysis, glucose metabolism

Introduction

Traditionally, $1\alpha,25(\text{OH})_2\text{VD}_3$ is a well-known steroid hormone for its crucial functions regulating mineral ion homeostasis in mammals (1–3). In zebrafish, a model teleost fish, $1\alpha,25(\text{OH})_2\text{VD}_3$ has been suggested to be involved in amino acid metabolism, inner ear and heart development, calcium handling, and cartilage development (4–10). In zebrafish

mutants with deficient in *cyp2r1*, an enzyme involved in vitamin D₃ activation, fatty acid oxidation in visceral adipose tissue (VAT) is promoted by 1 α ,25(OH)₂VD₃ in our laboratory (8). Recently, Shao et al. (2022) revealed the role of 1 α ,25(OH)₂VD₃ in the regulation of insulin and glucose metabolism with *cyp2r1*-deficient models (11). These studies indicated the diversity of physiological functions of vitamin D₃ signaling developed over its long evolution.

The vitamin D₃ and the metabolites developed functional versatility in energy metabolism, innate immune and skeletal development during the evolution. The action of 1 α ,25(OH)₂VD₃ has been suggested to be mediated by the nuclear vitamin D receptor (VDR), which form as a heterodimer with the retinoid X receptor, through specific sequences (VDR responsive elements [VREs]) on its target genes (1). A single *vdr* gene has been reported in most mammals, but two *vdr* paralogs, *vdra* and *vdrb*, have been identified in teleost fish; these paralogs arose after a whole-genome duplication event in teleosts (12). The functional diversity in the role of these two zebrafish VDRs in craniofacial cartilage development has been reported using a morpholino-based knockdown approach (10). Intriguingly, potent mitogenic effects on embryonic and adult cardiomyocytes have been demonstrated *in vivo* in *vdra* and *vdrb* double-knockout zebrafish, without effects on calcium handling, as stated recently (9). The metabolic functions of the vitamin D₃ signaling was fascinating for the adipose tissue homeostasis and insulin action regulation. It was appealing to clarify the VDR functional diversity in the metabolic control using genome editing technology. Furthermore it is of interest to further clarify the effects of vitamin D₃ signaling on mineral ion homeostasis and nutrient metabolism *in vivo* in zebrafish *vdr* mutants.

In the liver the enzymes CYP2R1 and CYP27A1 (not in human) convert vitamin D₃ into 1,25(OH)₂D₃, which is the most stable vitamin D metabolite in serum. In the previous study, *cyp2r1*-deficient fish have moderate phenotypes in the skeletal system and craniofacial bones. The plasma levels of 1,25(OH)₂D₃ was significantly decreased however constitutive levels of 1,25(OH)₂D₃ still existed. To investigate the function of vitamin D₃ signaling in skeletal system development two independent *vdra*- and *vdrb*-deficient zebrafish strains were generated using CRISPR/Cas9. Here we examined the multiple steps of vitamin D₃ signaling to investigate the functional diversification of vitamin D₃. The physiological phenotypes were analyzed and compared with the previous *cyp2r1* ablation models. Intriguingly, the plasma levels of 1,25(OH)₂D₃ and the activity of Insulin signaling were promoted significantly in the VDRs ablation models. The objective of this study was to elucidate the underlying mechanisms of VD₃/VDRs action.

Materials and methods

Zebrafish maintenance

Zebrafish (AB strains) were raised in a circulating aquarium system at 28.5°C with a 14-h light/10-h dark rhythm according to standard procedures. The animals were fed newly hatched brine shrimp (*Artemia salina*) three times at 8 am, 1 pm and 7 pm. Embryos were obtained through natural spawning and cultured at 28.5°C in egg water containing 0.006% ocean salt. The developmental

stages of embryos were determined as previously described (13). Since the present study were performed using the adult zebrafish. To avoid ovulation cycle bias on lipid and glucose metabolism, the male zebrafish was used only in the study. All fish experiments were conducted in accordance with the Guiding Principles for the Care and Use of Laboratory Animals and were approved by the Institute of Hydrobiology, Chinese Academy of Sciences (Approval ID: IHB2013724).

Establishment of *vdra* and *vdrb* knockout lines

The *vdra* and *vdrb* knockout lines were generated using CRISPR/Cas9 technology (14). Guide RNAs were designed using an online software tool (15) and were transcribed from PCR products. PCR products introduced a T7 promoter and gDNA sequence in the primer using the pMD19T-gRNA backbone plasmid as template. Followed purification using gel extraction kit the PCR products were used for gRNA synthesis using the TranscriptAid T7 High Yield Transcription Kit following the manufacturer's constructions (K0441, Thermo Fisher Scientific, Waltham, MA, USA). Cas9 mRNA was synthesized from the pXT7-Cas9 plasmid using the T7 mMACHINE mRNA Transcription Synthesis Kit (AM1344, Thermo Fisher Scientific) and purified using RNeasy Mini Kit (#74106, Qiagen, Hilden, Germany). The Cas9 mRNA and gRNA for *vdra* or *vdrb* were combined (500ng/ul Cas9 mRNA, 50ng/ul gRNA) for microinjection immediately before use (16). For genotyping, the PCR products amplified from the genomic DNA of fish were run in PAGE gel after denaturation and annealing. The PAGE gel was stained with ethidium bromide for 15 min before UVB imaging. The homoduplexes and heteroduplexes were separated with heteroduplexes being slower in mobility (17). The primers used in this study were listed in Table 1.

Micro CT imaging and relative bone density measurement

A 100-day-old male zebrafish was treated with an anesthetic (MS-222) and wiped off the water. The zebrafish is then attached to the foam using medical tape and placed in a scanning room. Whole zebrafish were scanned using a Micro CT system (SkyScan 1276, Bruker, Germany). The camera type is XIMEA MH110XC-KK-TP and the pixel size is 17.420um. The voltage and current are 55kV and 200uA respectively. Each constant motion scan resulted in 4668 projections over 180° with an exposure time of 175 ms per projection. The exposure is 517 ms. Each zebrafish is imaged after two or three scans, covering the head, belly and tail. The three-dimensional (3D) images of the bones were obtained by Skyscan CTAn software (v.1.1.7, Skyscan CTAn, Kontich, Belgium). At least three adults in each genotype were scanned.

The 100-day-old zebrafish was anesthetized, the tissue was removed, and the spine, about 20-25 sections, was obtained. The spine were scanned using a Micro CT system (SkyScan 1276, Bruker, Germany). Each constant motion scan resulted in 686 projections. The parameters are consistent with Micro CT. Each spine is imaged

TABLE 1 The primers used in the study.

FOR GENOTYPING	NCBI accession No.	Forward primer(5' - 3')	Reverse primer(5' - 3')
<i>vdra</i>	NC_007134.7	CGGTGGACACCAAGCTGAACT	CTCCAGTAATTCGCTCCTCAGC
<i>vdrb</i>	NC_007117.7	GTGAGGGCTGCAAAGGCTTCTTCA	CCCCTGAGACTCCAGGTTAACTCA
FOR qPCR ANALYSIS			
<i>pgc1a</i>	XM_017357139.2	GATTGAGGAGAGCACAGT	TCACAAGTGTAGCGGTAG
<i>trpv6</i>	NM_001001849.2	GTCCCAAACATACAAAGGC	TGGTGGCAATAATCTCAA
<i>g6pca.1</i>	NM_001003512.2	TCCAAGTGGAGCATGACT	ATCCTGGTATTGATCTGTAAAG
<i>g6pca.2</i>	NM_001163806.1	TAGCAAAGGGAAGAAATCA	CTTTAGACTCGCACTGTAGAT
<i>pck1</i>	NM_214751.1	TGGAGGAGGAGTCAGTCAGC	CCACCACATACGGCGAGT
<i>chrebp</i>	KF713494.1	ACCCCGACATGACCTTCAAC	TGTGGCATCTCTGTGTTGCT
<i>insra</i>	NM_001142672.1	GCGTGGCAATAATCTGTTCT	CGTTGATAGTGGTGGGGGG
<i>insulin</i>	NM_131056.1	GGTCCTGTTGGTCGTGTC	GTTGTAGAAGAAGCCTGTTGG
<i>gck</i>	NM_001045385.2	TGATATTGTGCGTCTGGCGT	GCTGCCTTCTTGACTGGA
<i>glut2</i>	NM_001042721.1	ATGTCTTCATCGTTTTGCC	CAGCCTCTCTTGAGGTTG
<i>acsl1b</i>	NM_001003569.2	CTGACGAGTTCGGTCGAGTT	TGGCGTACCAGTATGCAGTG
<i>cpt1b</i>	NM_001328192.1	TGAGACGGATTCTTTCCGCT	TTCGCTAGGCTTGTTACTTGC
<i>cpt2</i>	NM_001007447.1	AATGGATTGGGTGCAACGTG	TGAGTTCTAACCTTCAGGCTCT
<i>lpl</i>	NM_131127.1	GGACGGTCACGGGTATGTTT	CGATTCTGCAACATGAGCG
<i>fads2</i>	NM_131645.2	CCAATCAGAGCGAGCCTTCA	ACGCATTCAAAGTGCCACAA
<i>acc</i>	NM_001271308.1	ATGGCAGAGCAAGACTCCAC	CCTCTGCAGGTCGATACGTC
<i>elovl5</i>	NM_200453.2	TTTCGGCTAGAAGAAAGCAGT	GAACCGAAAGTGGGAGGTG
<i>ppar-gama</i>	NM_131467.1	AGCGACAATGCTCCTTTT	CACITCGATGACCCCGTA
<i>scd</i>	NM_198815.2	CCGACCCTCACAACCTCAAACC	GACAACGAAGCACATCAACACC
<i>cyp2r1</i>	NM_001386362.1	GACACCTTTGCCATTAT	CAGAAGTCTCCCATTTT
<i>cyp24a1</i>	NM_001089458.1	AAAGAGGGCAGCTATCCTGA	CATGAGCTTCTGCTGAAAG
<i>cyp27b1</i>	NM_001311791.1	AAGCCGTCGTCAAGGAAAT	CTCAGACGTGGCGTAATGA
<i>β-actin</i>	NM_131031.1	ACTCAGGATGCGGAACTGG	AGGGCAAAGTGGTAAACGCT
<i>ef1α</i>	NM_131263	TACCCTCTCTTGGTCGCTTT	ACCTTTGGAACGGTGTGATTG

after two scans. The Skyscan CTAn software was used to calculate the bone density of each section and the bone density of all sections of the spine was averaged. At least three adults in each genotype were scanned.

Total RNA extraction and quantitative real-time PCR

The gill, adipose tissue and liver were dissected from zebrafish under the anaesthetic. Total RNA was extracted with 100mg gill, 60mg adipose tissue and 100mg liver tissue dissected 100-day-old male zebrafish in 1ml TRIzol reagent (Ambion, Austin, TX). Generally, RNA with a content of 1-3ug is used for cDNA synthesis. The cDNAs were synthesized using the Reverse Aid

First-Strand cDNA Synthesis Kit (K1622, Thermo Scientific, Waltman, MA, USA) according to the manufacturer's instructions. Quantitative real-time PCR primers were designed using "primer blast" in the National Center for Biotechnology Information (NCBI) database, and are listed in Table 2. The primers for qPCR were validated by DNA sequencing and agarose gel electrophoresis of PCR products. RT-qPCR was conducted using TransStart® Tip Green qPCR SuperMix (Transgen, China) with the Bio-Rad (CFX96 Touch) software. All mRNA levels were calculated as fold expression relative to the housekeeping gene, β -actin. Each sample was run in triplicate repeats and the results were calculated according to the method described previously (18). In order to avoid post-feeding interference, no feeding was performed from 4 pm the previous day until 8 am next day. All of the following genes were used the tissues of zebrafish in the fasting state except the chrebp and gck.

TABLE 2 The levels of $1\alpha,25(\text{OH})_2\text{VD}_3$ and free fatty acid.

TEST	Sample or treatment	Con	vdra-/-;vdrb-/-	vdra-/-	vdrb-/-
1,25(OH) ₂ VD ₃	Plasma(pg/ml)	161.0 ± 8.936a	480.3 ± 43.00c	259.6 ± 30.33b	345.9 ± 42.02b
	Liver(pg/g)	218.6 ± 2.005a	1633.0 ± 69.69c	352.8 ± 21.12b	409.8 ± 46.77b
	Adipose(pg/g)	657.8 ± 10.64a	69.4 ± 4.342c	456.9 ± 12.79b	130.2 ± 6.11c
Free Fatty Acid	Plasma(μmol/L)	721.5 ± 50.9a	780.1 ± 55.65a	845.3 ± 69.85a	777.1 ± 66.85a

* n=3 groups, 15-20 fish/group.

Mineral content measurement

Plasma of 100-day-old male zebrafish were used for nitration with nitric acid (HNO₃). The lysate was then diluted to 10 mL with 2% nitric acid solution. The calcium and phosphorus levels were measured using inductively coupled plasma-optical emission spectroscopy (ICP-OES) on a Perkin-Elmer Optimal 8000 (Perkin Elmer, MA, USA). ICP-OES calibration standards were prepared from stock solutions on a gravimetric basis. Three target calibration standards were used for each ion, and 2% HNO₃ in double-deionized water was used as a control.

Whole-mount *in situ* hybridization

The experiment was carried out according to Chou's method (19). Zebrafish gills were fixed with 4% paraformaldehyde overnight at 4°C, and then washed several times with phosphate-buffered saline (PBS). Fixed samples were rinsed with PBST (PBS with 0.2% Tween 20, 1.4 mmol l⁻¹ NaCl, 0.2 mmol l⁻¹ KCl, 0.1 mmol l⁻¹ Na₂HPO₄, and 0.002 mmol l⁻¹ KH₂PO₄; pH 7.4). After a brief washing with PBST, gill filaments were incubated with hybridization buffer (HyB) containing 60% formamide, 5x SSC, and 0.1% Tween 20 for 5 min at 65°C. Prehybridization was performed in HyB+ (the hybridization buffer supplemented with 500 μg ml⁻¹ yeast tRNA and 50 μg ml⁻¹ heparin) for 2 h at 65°C. After prehybridization, samples were hybridized in 100 ng of the RNA probe in 200 μl of HyB+ at 65°C overnight. Gills were then washed at 65°C for 10 min in 75% HyB and 25% 2x SSC, for 10 min in 50% HyB and 50% 2x SSC, for 10 min in 25% HyB and 75% 2x SSC, for 10 min in 2x SSC, and twice for 30 min each in 0.2x SSC at 70°C. Further washes were performed at room temperature for 5 min in 75% 0.2x SSC and 25% PBST, for 5 min in 50% 0.2x SSC and 50% PBST, for 5 min in 25% 0.2x SSC and 75% PBST, and for 5 min in PBST. After serial washings, gill filaments were incubated in blocking solution containing 5% sheep serum and 2 mg ml⁻¹ BSA in PBST for 2 h and then incubated in the 1:10 000 - diluted alkaline phosphatase-conjugated anti-dig antibody for another 16 h at 4°C. After the reaction, samples were washed with PBST plus blocking reagent and then stained with NBT and BCIP.

Nile Red staining

Nile Red (N3013; Sigma Aldrich, St. Louis, MO, USA) was dissolved in acetone at 1 mg/mL as the stock solution. Mutants and size-matched control zebrafish were immersed in system water containing 0.1 μg/mL Nile Red for 1 hr for larval fish. Images were

obtained using an Olympus SZX16 FL Stereo Microscope (Olympus, Tokyo, Japan) at an excitation wavelength of 488 nm.

Body fat ratio assay

Twelve adult zebrafish were selected randomly from the three mutant lines and controls. All samples were frozen in liquid nitrogen and put into the -80°C refrigerator overnight. Subsequently, the samples were lyophilized in vacuum drying equipment at -20°C for 24 h. Bodyweight was recorded before fat extraction in methanol and chloroform. The oil extracted from each fish was weighed. The total oil weight/dry body weight ratios were calculated.

Measurement of triglyceride, glycogen, lactic acid and free fatty acid

The triglyceride, glycogen, lactic acid levels in the livers of 100-day-old male zebrafish were measured using the Triglyceride Assay Kit (Item No. A110-1-1), Liver/Muscle Glycogen Assay Kit (Item No. A043-1-1), Lactic Acid Assay Kit (Item No. A019-2-1) purchased from Nanjing Jiancheng Bioengineering Institute. The tail of the zebrafish was cut off after anesthesia, and blood was collected from the severed tail with a micropipette gun rinsed with heparin sodium. Then the zebrafish was dissected to collect liver tissue. Each parallel sample required about 15mg of liver tissue or 10ul of plasma for the corresponding indicator detection. At least 3 parallel samples are required for each indicator. The detection kit for lactic acid in plasma is consistent with the detection kit for lactic acid in liver. The plasma FFA levels were measured using the Nonesterified Free fatty acids assay kit (Item No. A042-2-1) purchased from Nanjing Jiancheng Bioengineering Institute. The samples were processed following the procedure provided by the manufacturer. Each parallel sample required 4 ul of plasma, and the experiment was repeated eight times.

Measurement of $1\alpha,25(\text{OH})_2\text{VD}_3$ levels

Plasma was prepared from blood for measurement of $1\alpha,25(\text{OH})_2\text{VD}_3$ levels. $1\alpha,25(\text{OH})_2\text{VD}_3$ (Item No. D1530-10UG) and 4-phenyl-1,2,4-triazolin-3,5-dione (Item No. 42579-100MG) were purchased from Sigma Aldrich and used as standards. $1\alpha,25(\text{OH})_2\text{VD}_3$ was extracted from plasma and measured as according to a previous report (8) using ultra-performance liquid chromatography-triple quadrupole mass spectrometry (UPLC-TQMS) (ACQUITY UPLC System; Waters Corp, Milford, MA, USA). Quantification was

performed using calibration curves generated with the $1\alpha,25(\text{OH})_2\text{VD}_3$ standard. Calibrations and sample measurements were performed in triplicate.

Blood glucose measurement

The OneTouch UltraVue (LifeScan, Inc., Milpitas, CA, USA) glucometer was used for the measurement of blood glucose. Zebrafish were fed regularly with a chow diet and then fasted for 18 h prior or were fed normally for 2 h prior to removal of blood using a heparin-rinsed micropipette tip, as described previously (20). Student's *T*-test was used to evaluate blood glucose levels at different time points.

Western blotting

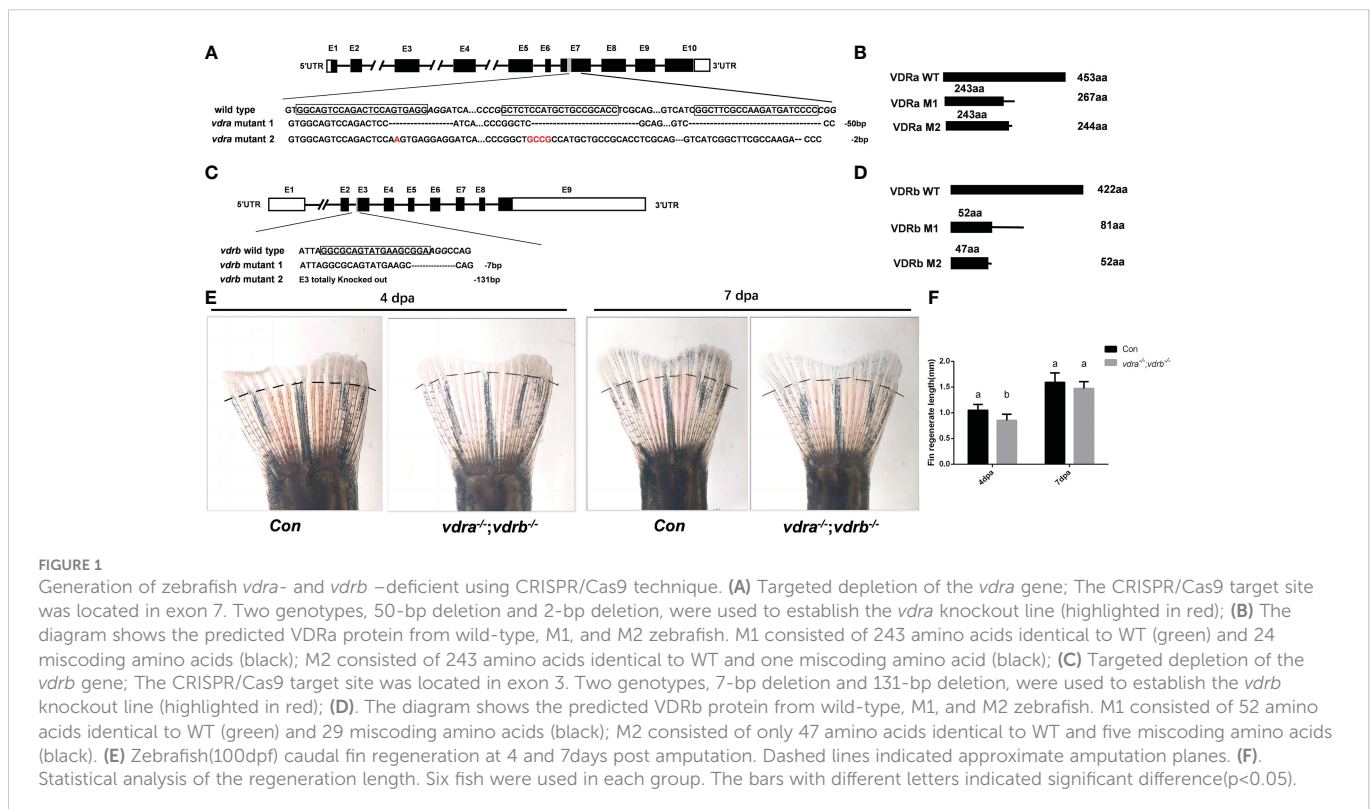
Protein samples were collected from the liver tissue of zebrafish at 100 dpf. The total protein of the liver tissue was extracted from 100mg liver tissue in 500 micro liter lysis buffer for each sample. For western blot analyses, sodium dodecyl sulfate-polyacrylamide gel electrophoresis (SDS-PAGE) was prepared as previously described (21). Total protein was separated by SDS-PAGE and transferred onto polyvinylidene difluoride membranes (Bio-Rad). Primary antibodies including anti- β -actin (AC026; ABclonal Technology, Woburn, MA, USA), anti-Akt (9272S; Cell Signaling Technology, Inc., Danvers, MA, USA), anti-phospho-Akt (Ser473) (4060S; Cell Signaling Technology, Inc.), anti-S6 ribosomal protein 5G10 (2217S; Cell Signaling Technology, Inc.) and anti-phospho-S6 (Ser235/236) (4858S; Cell Signaling Technology, Inc.) were diluted at 1:1,000 in

Can Get Signal antibody dilution solution (NKB-101; Toyobo Co., Ltd., Osaka, Japan). Signal was detected using a charge-coupled device camera-based imager (ImageQuant LAS 4000 mini; GE Healthcare, Chicago, IL, USA). The intensity of the bands was quantified using ImageJ version 1.49V (22) with β -actin, S6, or AKT serving as controls.

Results

Generation of zebrafish *vdra* and *vdrb* deficient using CRISPR/Cas9 technique

To investigate the function and regulation mechanisms of VD_3/VDR signaling, *vdra* and *vdrb* were knocked out using CRISPR/Cas9. The target of CRISPR/Cas9 for *vdra* was located in exon 7, and target of the CRISPR/Cas9 for *vdrb* was located in exon 3. F_0 embryos were injected with Cas9-mRNA and guide RNA (gRNA). Genomic DNA were extracted from some of the injected F_0 embryos for genotyping. The remaining F_0 embryos were allowed to develop and reproduce. The F_1 generation was genotyped and deep sequenced. Then, two mutant lines for *vdra* and *vdrb* were established. The altered genetic sequences of *vdra* and *vdrb* are shown in Figures 1A, C. The mutant genomic sequences of *vdra* and *vdrb* alleles produced premature proteins (Figures 1B, D). Since there was low universality of the mammal VDR antibody to detect zebrafish VDRs protein. The fin regeneration was examined and the phenotype was verified accordance with previous investigation (Figures 1E, F). Vitamin D receptors ablation inhibited regeneration of amputated fins as previously described.



Nuclear receptors of VD₃ is not essential for calcium homeostasis in zebrafish

Vitamin D₃, in particular its active metabolite 1 α ,25(OH)₂VD₃, is widely known as a modulator of calcium and phosphate homeostasis. Deficiency in VD₃ or VDR signaling will cause impaired bone mineralization. To further determine whether VDRs are necessary for calcium, phosphate homeostasis and mineralization of the bone, micro-computed tomography (CT) imaging was performed. The images showed that there were no significant defects in the mineralization of the vertebral column, ribs, craniofacial bone and fins in VDR mutants (Figure 2A). The relative skeletal bone density was examined and calculated. There were no significant difference between *vdra*^{-/-};*vdrb*^{-/-}, *vdra*^{-/-}, *vdrb*^{-/-} and control zebrafish although the bone density of *vdra*^{-/-};*vdrb*^{-/-} was moderately decreased (Figure 2B). Calcium and phosphate levels were also not significantly changed compared with controls (Figures 2C, D). The calcium transporter protein TRPV6, of which the promoter contains a VDR element, served as a 1 α ,25(OH)₂VD₃/VDR target gene. Expression levels of *trpv6* were checked using real-time PCR. Corresponding with calcium levels, the expression of *trpv6* was retained in the gills. The expression of *trpv6* was even enhanced in *vdra*^{-/-};*vdrb*^{-/-} and *vdrb*^{-/-} fish (Figure 2E). For better view of *trpv6* expression pattern in gills, *in situ* hybridization was performed. According with the relative quantification data, the *trpv6* expression was increased in the *vdrb* ablation and *vdra*^{-/-}; *vdrb*^{-/-} double knockout fish (Figures 2F–I).

Growth retardation and accumulated adiposity in the *vdra*^{-/-}; *vdrb*^{-/-} zebrafish

Our previous study demonstrated that 1 α ,25(OH)₂VD₃ was required for lipid metabolism and adipose tissue homeostasis (8). 1 α ,25(OH)₂VD₃ deficiency caused by knockout of *cyp27b1* gave rise to drastic growth retardation. In the present study, *vdra*-deficient zebrafish showed slightly reduced growth, while *vdrb*-deficient zebrafish showed normal growth compared with controls (Figures 3A–E). The double knockout of *vdra* and *vdrb* exhibited more severe growth retardation because of elimination of functional redundancy (Figures 3A–E). Besides the features of lipid metabolism in *vdr*-deficient fish were analyzed. The whole mount triglyceride levels of adult *vdra*^{-/-};*vdrb*^{-/-} zebrafish was significantly higher compared with control zebrafish (Figure 3F). As a main location of lipid metabolism, triglyceride levels in the liver were measured. Consistent with the TG content in the entire body, *vdra*^{-/-};*vdrb*^{-/-} fish exhibited higher triglycerides in the liver compared with the controls (Figure 3G). The Nile-Red-stained visceral fat of larvae fish was viewed using stereoscope with size-matched

mutant fish and control fish. The visceral adipose tissue significantly increased in *vdra*^{-/-};*vdrb*^{-/-} line compared with control fish (Figure 3H). Therefore, the *vdra*^{-/-};*vdrb*^{-/-} line, in which the 1 α ,25(OH)₂VD₃ nuclear receptor was substantially deficient, served as the main model used in subsequent investigations.

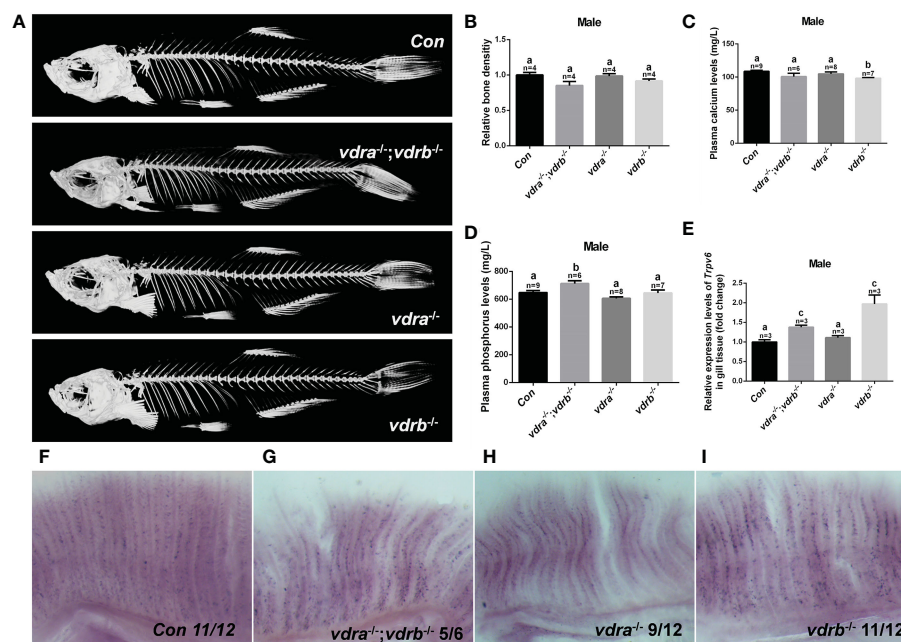


FIGURE 2

The activities of *vdra* and *vdrb* are dispensable for the calcium homeostasis and bone development. (A) Micro CT scanning images of mutants and control siblings at 100 dpf; (B) the relative bone density examined using CT scanning. (C) Calcium and (D) phosphorus levels in plasma were measured in mutants and control siblings at 100 dpf; (E) Quantitative real-time PCR assays show the *trpv6* transcript levels in the gills of mutants and control siblings at 100 dpf. (F–I). The *trpv6* expression patterns in the gill of the mutant and control. The representative images were selected and the blue-purple dot in the gills was the expression signals. The bars with different letters indicated significant difference ($p < 0.05$).

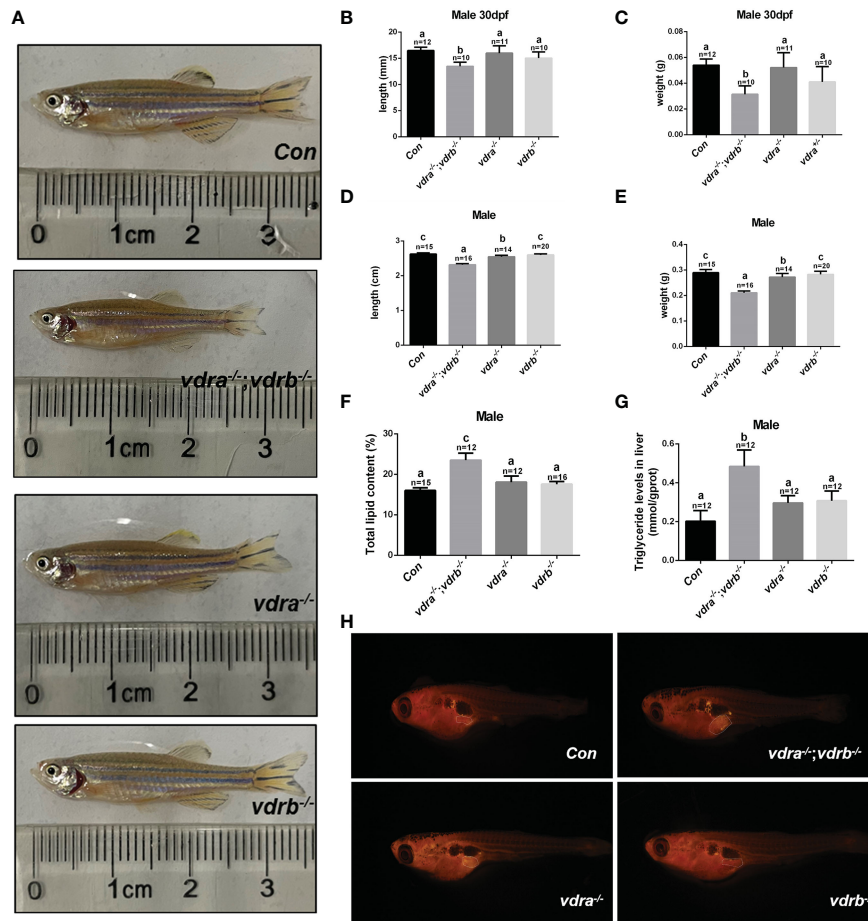


FIGURE 3

Retarded growth and accumulated adiposity observed in *vdra*^{-/-};*vdrb*^{-/-} zebrafish. (A) Comparison of the morphological features of mutants and control siblings at 100 dpf; (B–E) The body length and weight of the mutant lines and control siblings. (B, C) showed the zebrafish at 30 dpf and (D, E) showed the zebrafish at 100 dpf. (F) The total lipid levels of male mutants and controls at 100 dpf; controls, n = 15; *vdra*^{-/-};*vdrb*^{-/-}, n = 12; *vdra*^{-/-};*vdrb*^{+/-}, n = 12; *vdra*^{+/-};*vdrb*^{-/-}, n = 16; (G) The levels of triglycerides in the liver of mutants and control siblings at 100 dpf; (H). Neutral lipids of juvenile mutants and size-matched controls (both with a standard length of 7.6 mm) were stained with Nile Red and viewed with stereoscope. The visceral adipose tissue was labeled by the surrounded dashed line. The bars with different letters indicated significant difference (p < 0.05).

VDRs ablation impair lipid and glucose homeostasis in liver and adipose tissue

Since the observation of the fatty liver and increased visceral adiposity, we checked the lipid metabolism state in liver and adipose tissue. The free fatty acid (FFA) was measured and there was no significant difference between *vdra*^{-/-};*vdrb*^{-/-} line and control line (Table 2). Δ -6-fatty acid desaturase (*fads2*) is the key enzyme in the biosynthesis of polyunsaturated fatty acids (PUFAs). *Acetyl-CoA carboxylase* (ACC) is a biotin-dependent enzyme that catalyses the irreversible carboxylation of acetyl-CoA to malonyl-CoA, the rate-limiting step in fatty acid biosynthetic pathway. *Elongases of very long-chain fatty acids 5* (*elovl5*) are the initial and rate-limiting enzymes responsible for the condensation of activated fatty acids with malonyl-CoA required for biosynthesis of long-chain fatty acids. *Peroxisome proliferator-activated receptor gamma* (*ppar* γ) as the lipid synthesis regulator, enhanced lipogenesis through upregulation of at both transcript and protein levels. *Stearyl-CoA desaturase* (SCD) is known for their roles in synthesizing unsaturated fatty acids. The lipogenesis pathway was enhanced in the liver with the elevated transcription levels

of *fads2*, ACC and *elovl5*. While in the adipose tissue the lipogenesis pathway was suppressed with the decreased transcription levels of *fads2*, ACC, *elovl5* and *ppar* γ (Figures 4A, C). Carnitine palmitoyltransferase (CPT) catalyze the conversion of fatty acylCoAs into fatty acylcarnitines for entry into the mitochondrial matrix, it is deemed as the main regulatory enzyme in mitochondrial fatty acid β -oxidation. The expression of *pgc1 α* , which is a modulator of beta-oxidation, was significantly suppressed (Figures 4B, D). The lipolysis pathway was down-regulated in the adipose and liver tissue with the decreased transcription levels of *cpt1b*, *cpt2*, and *pgc1 α* . The mitochondria uncoupling proteins were belonged to super mitochondria carrier superfamily with a general role in protection against oxidative stress. And the *ucps* were stimulated by fatty acid oxidation. The transcript levels of some mitochondria-related genes, such as *ucp1* (uncoupling protein 1) and *ucp2* (uncoupling protein 2) were suppressed (Figures 4B, D). This suggested that the elevated triglyceride accumulation in adipose tissue was attributed to defects in triglyceride mobilization. While in the liver the beta-oxidation was suppressed and lipogenesis was promoted.

In the previous investigation, $1\alpha,25(\text{OH})_2\text{VD}_3$ signaling regulates insulin signaling through modulating the expression of the insulin

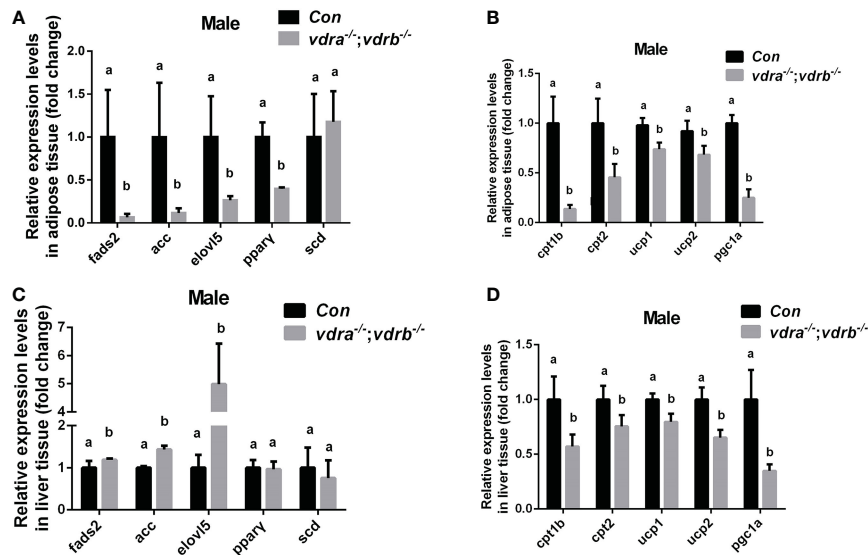


FIGURE 4

Transcriptional levels of marker genes involved in the lipogenesis and lipid oxidation. (A, C) Relative expression levels of marker genes involved in lipogenesis including *fads2*, *acc*, *elov15*, *ppary* and *scd* in adipose tissue (A) and liver tissue (C) of mutant line and control. Three biological repeats were carried out and statistical analysis was performed using a t test ($n=3$). (B, D) Relative expression levels of *cpt1b*, *cpt2*, *ucp1*, *ucp2* and *pgc1a* in adipose tissue (A) and liver tissue (C) of mutant line and control. Three biological repeats were carried out and statistical analysis was performed using a t test ($n=3$). There was no difference between the two internal reference gene (β -actin and *EF1a*). The bars with different letters indicated significant difference ($p<0.05$).

receptor. $1\alpha,25(\text{OH})_2\text{VD}_3$ -deficient zebrafish exhibited impaired blood glucose homeostasis and hyperglycemia (11). Therefore the blood glucose levels of VDRs ablation zebrafish were checked. The fasting blood glucose levels were indistinguishable between the control zebrafish and the *vdra*^{-/-};*vdrb*^{-/-} zebrafish. However the postprandial blood glucose levels of the *vdra*^{-/-};*vdrb*^{-/-} line was decreased compared with control line (Figure 5A). The data suggested that the glucose tolerance was ameliorated in the *vdra*^{-/-};*vdrb*^{-/-} zebrafish. This speculation was supported by the increased expression of *glut2* and *gck*, which are markers for glycolysis and glucose transportation into cells (Figures 5B, C). The expression of *chrebp*, which encodes a key positive regulator of lipid synthesis, was increased (Figure 5D). This suggested that lipid synthesis from glucose was promoted in the liver. Although there was increased glycolysis, gluconeogenesis was unaffected (Figure 5E). The expression levels of key regulators and enzymes of gluconeogenesis such as *pck1*, *g6pca.2*, and *g6pca.1* in the liver were unaffected in *vdra*^{-/-};*vdrb*^{-/-} fish (Figure 5E). To determine effects on the metabolic pathways of glucose, metabolites such as glycogen and lactic acid were measured. The synthesis of lactic acid and glycogen were elevated in the liver, which revealed increased liver glucose catabolism (Figures 5F–H).

Elevated $1\alpha,25(\text{OH})_2\text{VD}_3$ levels and Enhanced insulin signaling activity in the *vdra*^{-/-};*vdrb*^{-/-} zebrafish

To investigate the mechanisms of VDR involvement in insulin signaling, $1\alpha,25(\text{OH})_2\text{VD}_3$ levels were monitored using ultra high-performance liquid chromatography-triple quadrupole mass

spectrometry (UPLC-TQMS). The levels of $1\alpha,25(\text{OH})_2\text{VD}_3$ were significantly elevated compared with controls in the plasma and liver (Table 2). However the levels of $1\alpha,25(\text{OH})_2\text{VD}_3$ in the adipose tissue was significantly suppressed. It has been suggested that ablation of the VDRs would promote ligand production as a feedback effect. The major enzyme encoding genes responsible for $1\alpha,25(\text{OH})_2\text{VD}_3$ homeostasis including *cyp2r1*, *cyp27b1* and *cyp24a1* were tested. The expression of *cyp24a1* was significantly reduced. The expression of *cyp27b1* was suppressed. However the expression of *cyp2r1* which was responded for $25(\text{OH})\text{VD}_3$ synthesis was substantially promoted (Figure 6A). Intriguingly, the expression levels of insulin and insulin receptor were significantly increased in the liver of *vdra*^{-/-};*vdrb*^{-/-} zebrafish (Figures 6B, C). Due to the increased insulin signaling and $1\alpha,25(\text{OH})_2\text{VD}_3$ levels, the activity of the AKT/mTOR pathway was also measured, showing increased levels of phosphorylated AKT and S6 proteins (Figures 6D, E). In summary, *vdra*^{-/-};*vdrb*^{-/-} zebrafish showed elevated $1\alpha,25(\text{OH})_2\text{VD}_3$ levels in the liver, and this promoted insulin/insulin-receptor signaling. Therefore, the augmentation of insulin activity enhanced glucose absorption and lipid synthesis.

Discussion

Insights into the physiological actions of $1\alpha,25(\text{OH})_2\text{VD}_3$ in zebrafish have been gradually achieved from recent studies in several deficient zebrafish models (5–11). Basically, the involvement of $1\alpha,25(\text{OH})_2\text{VD}_3$ in mineral ion homeostasis or related craniofacial cartilage development in zebrafish have been only observed in several studies using morpholino-based knockdowns (5, 10). However, no effects on physiological calcium handling have been seen in several

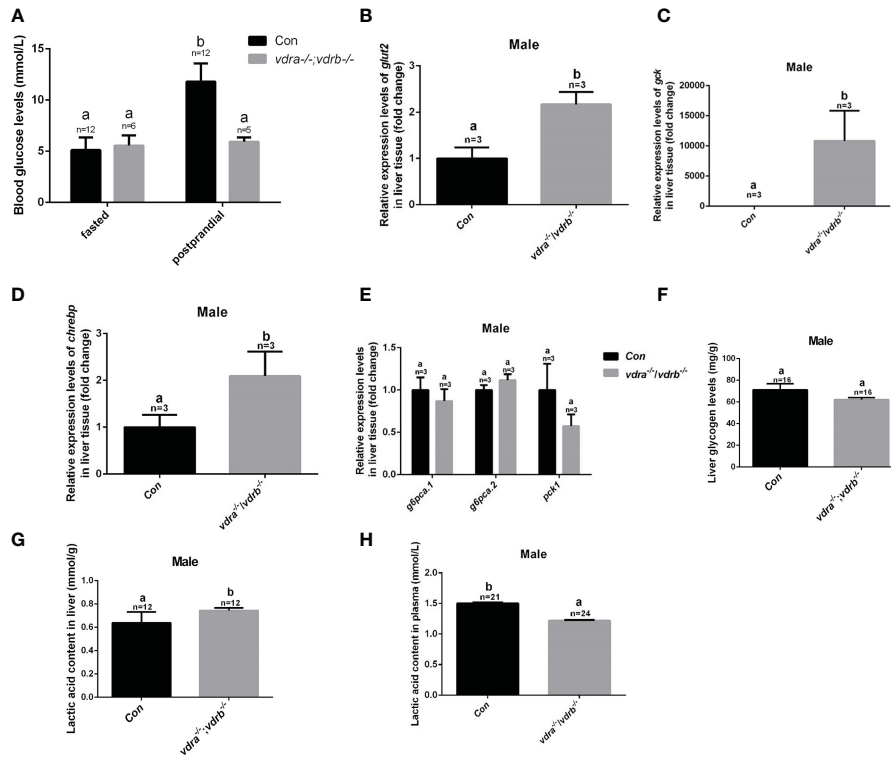


FIGURE 5 Glucose metabolic homeostasis was impaired in the liver of *vdra*^{-/-};*vdrb*^{-/-} zebrafish. (A) Blood glucose levels of *vdra*^{-/-};*vdrb*^{-/-} fish and control siblings in the fasted state and postprandial state at 100 dpf. (B–D). Quantitative real-time PCR showed *glut2*, *gck* and *chreb* transcriptional levels in the liver of mutants and control siblings at 100 dpf; (E) Quantitative real-time PCR showed gluconeogenesis marker gene *g6pca.1*, *g6pca.2* and *pck1* transcriptional levels in the liver of the *vdra*^{-/-};*vdrb*^{-/-} fish and control siblings at 100dpf. (F) The liver glycogen levels in *vdra*^{-/-};*vdrb*^{-/-} fish and control siblings at 100 dpf. (G, H). The liver lactic acid levels in *vdra*^{-/-};*vdrb*^{-/-} fish and control siblings at 100 dpf. The bars with different letters indicated significant difference (p<0.05).

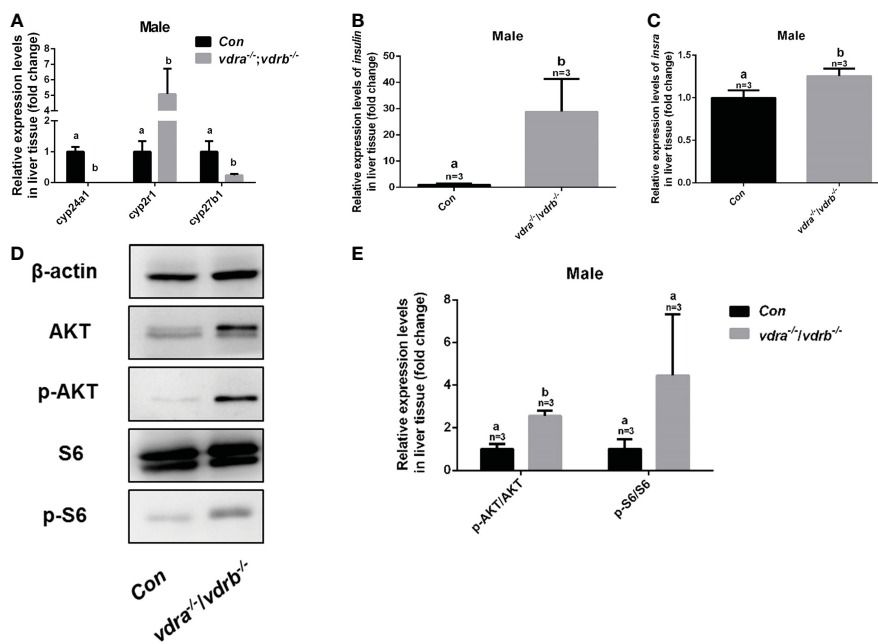


FIGURE 6 Enhanced insulin signaling observed in *vdra*^{-/-};*vdrb*^{-/-} zebrafish. (A) Quantitative real-time PCR showed the *cyp24a1*, *cyp2r1* and *cyp27b1* transcript levels in the liver of *vdra*^{-/-};*vdrb*^{-/-} fish and control siblings at 100 dpf; (B, C) Quantitative real-time PCR showed the *insulin* and *insra* transcriptional levels in the liver of *vdra*^{-/-};*vdrb*^{-/-} fish and control siblings at 100 dpf; (D) AKT, p-AKT, S6, and p-S6 protein levels in liver samples of *vdra*^{-/-};*vdrb*^{-/-} fish and control siblings at 100 dpf; (E) Quantification of relative p-AKT/AKT and p-S6/S6 protein levels from western blot analysis.

$1\alpha,25(\text{OH})_2\text{VD}_3$ signaling-deficient zebrafish models (8, 9), which is similar to the phenotypes seen in the present study. This suggests that calcium homeostasis might not necessarily be dependent on the nuclear VDR in teleosts.

Surprisingly, no significantly defective calcium homeostasis or skeletal development was seen in *cyp2r1*-deficient (8) and *vdra*^{-/-}; *vdrb*^{-/-} zebrafish (Figure 2). Moreover, no such defects has been stated in other *vdra*^{-/-}; *vdrb*^{-/-} zebrafish model either (9). The *trpv6* was reported to be the downstream effector of vitamin D₃/VDR signaling. The expression of *trpv6* in the gill was upregulated in *vdra*^{-/-}; *vdrb*^{-/-} and *vdrb*^{-/-} zebrafish. It indicated that the *trpv6* expression induction was VDRs independent. In the $1\alpha,25(\text{OH})_2\text{VD}_3$ deficient model the *trpv6* expression was not affected both larval and adult stage. the vitamin D₃/VDR signaling was not essential for the Ca²⁺ absorption in teleost fish. Both VDRa and VDRb were functional redundant. Double knockout of the VDRs caused more severe growth retardation and adiposity. However, similar phenotypes regarding retarded growth, increased obesity, and decreased *pgc1 α* expression have been seen in both *cyp2r1*^{-/-} and *vdra*^{-/-}; *vdrb*^{-/-} zebrafish (8). The involvement of $1\alpha,25(\text{OH})_2\text{VD}_3$ signaling in fatty acid metabolism has also been reported (4, 23). The levels of $1\alpha,25(\text{OH})_2\text{VD}_3$ were significantly elevated in *vdra*^{-/-}; *vdrb*^{-/-} zebrafish due to a feedback mechanism. The mitochondria beta oxidation related genes were suppressed significantly in the *vdra*^{-/-}; *vdrb*^{-/-} zebrafish. Therefore, the decreased lipid oxidation can be attributed to the impaired downstream VDR signaling.

In zebrafish, two types of nuclear VDRs have been identified (12). Compared with the differences between the *cyp2r1*^{-/-} zebrafish and *vdra*^{-/-}; *vdrb*^{-/-} zebrafish in terms of the body weight and length, milder defects were seen in *vdra*^{-/-}; *vdrb*^{-/-} fish compared to control siblings at 100 days post-fertilization (8). Considering that about half of the plasma content of $1\alpha,25(\text{OH})_2\text{VD}_3$ still remained in *cyp2r1*^{-/-} zebrafish (8), it is reasonable to speculate that vitamin D₃ signaling can act in a nuclear VDR-independent manner. Intriguingly, decreased insulin levels were seen in *cyp2r1*^{-/-} zebrafish with reduced $1\alpha,25(\text{OH})_2\text{VD}_3$ levels (11). However, significant upregulation of insulin transcriptional and AKT activation have been seen in the liver of the present *vdra*^{-/-}; *vdrb*^{-/-} zebrafish. A previous study, in which diet-supplemented vitamin D₃ could promote insulin signaling supports this speculation (11). Moreover, significant enhancement of glucose catabolism was also seen in our *vdra*^{-/-}; *vdrb*^{-/-} zebrafish. Augmentation of insulin signaling promoted glucose uptake, glycolysis and lipid synthesis revealed by the increased expression of *glut2*, *gck* and *chrebp*. In view of the elevated plasma levels of $1\alpha,25(\text{OH})_2\text{VD}_3$ presented in *vdra*^{-/-}; *vdrb*^{-/-} zebrafish, it could be promotion of the high levels of the $1\alpha,25(\text{OH})_2\text{VD}_3$ on insulin signaling with the receptor(s) other than VDRa or VDRb in zebrafish.

Protein disulfide isomerase family A member 3 (*pdia3*), also known as $1\alpha,25(\text{OH})_2\text{VD}_3$ -membrane-associated rapid response to steroid, has been described as a crucial protein in $1\alpha,25(\text{OH})_2\text{VD}_3$ -initiated rapid membrane non-genomic signaling pathways in mammals (24, 25). No significant alterations in transcriptional expression levels of *pdia3* were observed in the hepatic tissue of our *vdra*^{-/-}; *vdrb*^{-/-} fish (data not shown). However, the majority of the responses mediated by vitamin D₃ non-genomic signaling have implicated post-translational modification (24, 26, 27). It has been

reported that *pdia3* might have a significant role in calcium absorption, skeletal development, lipogenesis, and insulin regulation (24–27).

The lack of available data on the non-genomic actions of vitamin D₃ stands in the way of understanding the mode of actions of vitamin D₃ metabolites. Further studies will need to be performed to revealed the modes of action of vitamin D₃ across its evolutionary history using teleost models.

Conclusion

In the present study we utilized *vdra*^{-/-}; *vdrb*^{-/-} double knockout zebrafish model to characterize the function of VD₃/VDRs signaling. Our results demonstrated VDRs were nor essential for calcium homeostasis and skeleton development. The $1\alpha,25(\text{OH})_2\text{VD}_3$ levels were elevated through *cyp24a1* transcriptional repression. The lipolysis was not affected in the *vdra*^{-/-}; *vdrb*^{-/-} zebrafish. However the lipid oxidation activities were inhibited due to the VDRs ablation. Furthermore enhanced transcription level and activity of Insulin/Insr were achieved in the *vdra*^{-/-}; *vdrb*^{-/-} zebrafish. Augmentation of the glucose uptake, glycolysis and lipogenesis intensified the lipid accumulation in the liver.

Data availability statement

The original contributions presented in the study are included in the article/Supplementary Material. Further inquiries can be directed to the corresponding author.

Ethics statement

All animal experiments were conducted in accordance with the Guiding Principles for the Care and Use of Laboratory Animals and were approved by the Institute of Hydrobiology, Chinese Academy of Sciences (Approval ID: IHB 2013724).

Author contributions

RL conducted most of the experiments for this study. XP and YL provided guidance in experimental operation. XJ, JH, and GZ helped in maintaining the fish system technical guidance. QL and ZY performed training and provided insights for this work. QL and ZY wrote the paper and prepared the figures. ZY initiated and supervised the research team and edited the paper. JJ, YR, SS, TS, and TL gave valuable suggestion and discussion. All authors contributed to the article and approved the submitted version.

Funding

This project was supported by the National Key Research and Development Program of China [2022YFF100300]; National Natural Science Foundation, China [32172956 to QL].

Acknowledgments

We would like to thank Ms Guangxin Wang at The Analysis and Testing Center of Institute of Hydrobiology, Chinese academy of Sciences for the assistance for microscope photography.

Conflict of interest

The authors declare that the research was conducted in the absence of any commercial or financial relationships that could be construed as a potential conflict of interest.

References

1. Yan CL, Pirro AE, Amling M, Delling G, Baron R. Targeted ablation of the vitamin d receptor: An animal model of vitamin d-dependent rickets type II with alopecia. *Proc Natl Acad Sci* (1997) 94(18):9831–5. doi: 10.1073/pnas.94.18.9831
2. Rummens K, Cromphaut S, Carmeliet G, Herck EV, Bree RV, Stockmans I, et al. Pregnancy in mice lacking the vitamin d receptor: Normal maternal skeletal response, but fetal hypomineralization rescued by maternal calcium supplementation. *Pediatr Res*. (2003) 54:466–73. doi: 10.1203/01.PDR.0000081302.06915.D3
3. Cromphaut SV, Dewerchin M, Hoenderop J, Stockmans I, Carmeliet G. Duodenal calcium absorption in vitamin d receptor-knock out mice: functional and molecular aspects. *Anti-Cancer Drugs* (2002) 13(5):A4–4. doi: 10.1073/pnas.231474698
4. Craig TA, Zhang Y, McNulty MS, Middha S, Ketha H, Singh RJ, et al. Research resource: whole transcriptome RNA sequencing detects multiple $1\alpha,25$ -dihydroxyvitamin D(3)-sensitive metabolic pathways in developing zebrafish. *Mol Endocrinol* (2012) 26(9):1630. doi: 10.1210/me.2012-1113
5. Lin CH, Su CH, Tseng DY, Ding FC, Hwang PP. Action of vitamin d and the receptor, VDRa, in calcium handling in zebrafish (*Danio rerio*). *PLoS One* (2012) 7(9):e45650. doi: 10.1371/journal.pone.0045650
6. Kwon H-J. Vitamin d receptor deficiency impairs inner ear development in zebrafish. *Biochem Biophys Res Commun* (2016) 478(2):994–8. doi: 10.1016/j.bbrc.2016.08.070
7. Kwon H-J. Vitamin d receptor signaling is required for heart development in zebrafish embryo. *Biochem Biophys Res Commun* (2016) 470(3):575–8. doi: 10.1016/j.bbrc.2016.01.103
8. Peng X, Shang G, Wang W, Chen X, Lou Q, Zhai G, et al. Fatty acid oxidation in zebrafish adipose tissue is promoted by $1\alpha,25$ (OH) $2D_3$. *Cell Rep* (2017) 19(7):1444–55. doi: 10.1016/j.celrep.2017.04.066
9. Han Y, Chen A, Umansky KB, Oonk KA, Choi WY, Dickson AL, et al. Vitamin d stimulates cardiomyocyte proliferation and controls organ size and regeneration in zebrafish. *Dev Cell* (2019) 48(6):853–863.e5. doi: 10.1016/j.devcel.2019.01.001
10. Kwon HJ. Vitamin d receptor signaling regulates craniofacial cartilage development in zebrafish. *J Dev Biol* (2019) 7(2):13. doi: 10.3390/jdb7020013
11. Shao R, Liao X, Lan Y, Zhang H, Jiao L, Du Q, et al. Vitamin d regulates insulin pathway and glucose metabolism in zebrafish (*Danio rerio*). *FASEB J* (2022) 36(5):e22330. doi: 10.1096/fj.202200334RR
12. Kollitz EM, Beth HM, Kerr WG, Kullman SW. Functional diversification of vitamin d receptor paralogs in teleost fish after a whole genome duplication event. *Endocrinol* (2014) 12:en20141505. doi: 10.1210/en.2014-1505
13. Kimmel CB, Ballard WW, Kimmel SR, Ullmann B, Schilling TF. Stages of embryonic development of the zebrafish. *Dev dyn* (1995) 203(3):253–310. doi: 10.1002/aja.1002030302
14. Mali P, Yang L, Esvelt KM, Aach J, Guell M, DiCarlo JE, et al. RNA-Guided human genome engineering via Cas9. *Sci* (2013) 339(6121):823–6. doi: 10.1126/science.1232033
15. Sander JD, Zaback P, Joung JK, Voytas DF, Dobbs D. Zinc finger targeter (ZiFIT): an engineered zinc finger/target site design tool. *Nucleic Acids Res* (2007) 35(suppl_2):W599–605. doi: 10.1093/nar/gkm349
16. Hwang WY, Fu Y, Reyon D, Maeder ML, Tsai SQ, Sander JD, et al. Efficient genome editing in zebrafish using a CRISPR-cas system. *Nat Biotechnol* (2013) 31(3):227–9. doi: 10.1038/nbt.2501
17. Zhang Z, Zhu B, Ge W. Genetic analysis of zebrafish gonadotropin (FSH and LH) functions by TALEN-mediated gene disruption. *Mol Endocrinol* (2015) 29(1):76–98. doi: 10.1210/me.2014-1256
18. Bustin SA, Benes V, Garson JA, Hellemans J, Huggett J, Kubista M, et al. *The MIQE guidelines: Minimum Information for publication of quantitative real-time PCR experiments*. Oxford University Press (2009) 55(4):611–22. doi: 10.1373/clinchem.2008.112797
19. Chou M-Y, Hsiao C-D, Chen S-C, Chen I-W, Liu S-T, Hwang P-P. Effects of hypothermia on gene expression in zebrafish gills: upregulation in differentiation and function of ionocytes as compensatory responses. *J Exp Biol*. (2008) 211(19):3077–84.
20. Gao Y, Dai S, Shi C, Zhai G, Jin X, He J, et al. Depletion of myostatin b promotes somatic growth and lipid metabolism in zebrafish. *Front endocrinol* (2016) 7:88. doi: 10.3389/fendo.2016.00088
21. Shi C, Lou Q, Fu B, Jin J, Huang J, Lu Y, et al. Genomic polymorphisms at the *chrh2* locus improve feed conversion efficiency through alleviation of hypothalamus-pituitary-interrenal axis activity in gibel carp (*Carassius gibelio*). *Sci China Life Sci* (2022) 65(1):206–14. doi: 10.1007/s11427-020-1924-4
22. Schneider CA, Rasband WS, Eliceiri KW. NIH Image to ImageJ: 25 years of image analysis. *Nat Methods* (2012) 9(7):671–5. doi: 10.1038/nmeth.2089
23. Knuth MM, Mahapatra D, Jima D, Wan D, Hammock BD, Law M, et al. Vitamin d deficiency serves as a precursor to stunted growth and central adiposity in zebrafish. *Sci Rep* (2022) 10:16032. doi: 10.1038/s41598-020-72622-2
24. Donati S, Palmini G, Aurilia C, Falsetti I, Miglietta F, Iantomasi T, et al. Rapid nontranscriptional effects of calcifediol and calcitriol. *Nutrients* (2022) 14(6):1291. doi: 10.3390/nu14061291
25. Boyan BD, Sylvia VL, McKinney N, Schwartz Z. Membrane actions of vitamin d metabolites $1\alpha,25$ (OH) $2D_3$ and $24R,25$ (OH) $2D_3$ are retained in growth plate cartilage cells from vitamin d receptor knockout mice. *J Cell Biochem* (2003) 90(6):1207–23. doi: 10.1002/jcb.10716
26. Asano L, Watanabe M, Ryoden Y, Usuda K, Yamaguchi T, Khambu B, et al. Vitamin d metabolite, 25-hydroxyvitamin d, regulates lipid metabolism by inducing degradation of SREBP/SCAP. *Cell Chem Biol* (2017) 24(2):207–17. doi: 10.1016/j.chembiol.2016.12.017
27. Li N, Luo X, Yu Q, Yang P, Chen Z, Wang X, et al. SUMOylation of Pdia3 exacerbates proinsulin misfolding and ER stress in pancreatic beta cells. *J Mol Med* (2020) 98(12):1795–807. doi: 10.1007/s00109-020-02006-6

Publisher's note

All claims expressed in this article are solely those of the authors and do not necessarily represent those of their affiliated organizations, or those of the publisher, the editors and the reviewers. Any product that may be evaluated in this article, or claim that may be made by its manufacturer, is not guaranteed or endorsed by the publisher.

Supplementary material

The Supplementary Material for this article can be found online at: <https://www.frontiersin.org/articles/10.3389/fendo.2023.1054665/full#supplementary-material>